Enhancement in the performance of a quantum battery by ordered and disordered interactions

Srijon Ghosh,[1] Titas Chanda,[1,2] and Aditi Sen(De)[1]

[1]*Harish-Chandra Research Institute and HBNI, Chhatnag Road, Jhunsi, Allahabad 211019, India*

[2]*Instytut Fizyki im. Mariana Smoluchowskiego, Uniwersytet Jagielloński, Łojasiewicza 11, 30-348 Kraków, Poland*

(Received 5 January 2020; accepted 18 February 2020; published 23 March 2020)

Considering the ground state of a quantum spin model as the initial state of the quantum battery, we show that both ordered and disordered interaction strengths play a crucial role in increasing the extraction of power from it. In particular, we demonstrate that exchange interactions in the xy plane and in the z direction, leading to the XYZ spin chain, along with the local charging field in the x direction substantially enhance the efficiency of the battery compared to the model without interactions. Moreover, such an advantage in power obtained due to interactions is almost independent of the system size. We find that the behavior of the power, although measured during dynamics, can faithfully mimic the equilibrium quantum phase transitions present in the model. We observe that with the proper tuning of system parameters, an initial state prepared at finite temperature can generate higher power in the battery than that obtained with zero temperature. Finally, we report that defects or impurities, instead of reducing the performance, can create a larger amount of quenched averaged power in the battery in comparison with the situation when the initial state is produced from the spin chain without disorder, thereby showing the disorder-induced order in dynamics.

DOI: 10.1103/PhysRevA.101.032115

I. INTRODUCTION

In the modern era, devices which store energy for later purposes are extremely useful to fulfill our daily needs, ranging from communication appliances to medical accessories like artificial cardiac pacemakers and hearing aids. Prominent examples of such energy storage include batteries consisting of one or more chemical or electrochemical cells, converting chemical energy to electrical energy. They can be either disposable or rechargeable, and the the latter can be charged externally by using electricity and are very convenient due to their multiple usage facilities. On the other hand, it has been realized over the last few decades that technologies like computers and communication gadgets based on quantum mechanical principles can perform more efficiently than their classical analogs [1]. Importantly, such devices have already been built in laboratories using physical systems like photons, ion-traps, and superconducting qubits [2–12].

It is therefore natural to ask whether quantum mechanical properties like coherence [13] and entanglement [14] can also play a role in efficiently storing or generating energy. In this respect, two distinctly different versions of quantum batteries are proposed: (1) an arbitrary number of independent quantum systems acts as cells of a battery, and entangling unitary or nonunitary operations are applied for a suitable period to drive the system leading to the extraction of energy from it [15–25]; (2) the ground state of an interacting spin model can be considered as the initial state of the battery which can then be used as storage media where charging is performed via quantum mechanically allowed operations [26,27]. Although the former proposal has extensively been studied in recent years, the latter recently been explored and it was shown that the nature of the coupling of the initial ordered Hamiltonian is crucial for obtaining the improvement in the power [25]. In this paper, we concentrate on the second kind where the initial state of the battery is prepared in the ground or thermal state of the quantum spin chain and a *local* charging field is used to to drive the system required to extract power from the battery. With the development of ultracold atoms trapped in optical lattices or in trapped ions or in polar molecules, the basic ingredient for quantum battery, quantum many-body Hamiltonians, can currently be implemented and engineered in laboratories, thereby creating the possibility of manufacturing quantum technologies using these systems [4,8,28–31].

On the other hand, systems without any impurities or defects are in general difficult to build, and at the same time, keeping them at absolute zero temperature is also hard. Therefore, disordered systems [32–40] and effects of temperature on physical properties of many-body systems have attracted much attention recently [41–48]. Moreover, it was discovered that the disordered models posses exotic phases like Bose glass [49–52] (cf. Refs. [53–57]) which are not present in the homogeneous systems and can show counterintuitive phenomena like Anderson localization [32], many-body localization [58–62], and high-T_c superconductivity [63,64]. These disordered systems can also be created in a controlled manner in ultracold gases, and hence one can observe these phenomena and quantum phases in experiments, making this field more appealing [65–70].

In this paper, we first investigate the role of many-body interactions, ordered as well as disordered, of the parent Hamiltonian and the temperature of the initial state on the efficiency of the battery. Specifically, we show that in case of the transverse XY and the XYZ model without disorder, the power of the battery critically depends on the interactions and its characteristics like the ferromagnetic or the antiferromagnetic ones. We also find that the advantages

in power generation due to the interactions remain almost the same for different system sizes. Moreover, signatures of quantum critical points, present in these models, are clearly visible in the trends of the power. Note that although the output power of the battery is measured in the evolution of the system, it can still indicate the equilibrium property of the parent Hamiltonian (cf. Refs. [71,72]). We also show that suitable tuning of interactions and temperature lead to a situation where power of the quantum battery increases with the increase of temperature, although one intuitively expects that the initial state prepared at high temperature can destroy the effectiveness of the quantum battery. Moreover, we observe that the Gaussian-distributed random interaction strengths, both in the xy plane and in the z direction of the XYZ model, enhance the quenched-averaged power compared to that of the ordered case. Such counterintuitive phenomena were already demonstrated in physical quantities like magnetization, correlation length, and entanglement computed in the static scenario, i.e., in the ground or in the thermal states of the disordered models [73–92]. Our results indicate that such advantages can also be found in closed dynamics of the systems with defects.

The paper is organized as follows: In Sec. II we introduce the concept of a quantum battery and the respective measure to quantify its efficiency. We then discuss the quantum spin models, both ordered and disordered ones, that we use for modeling a quantum battery (Sec. III). We then present the results in Sec. IV for ordered spin models with the initial states of the battery being either the ground state or the thermal state with finite temperature. Finally, we show that models with random exchange interactions can increase the quenched averaged power of the battery in Sec. V. The conclusion is given in Sec. VI.

II. QUANTUM BATTERY BUILT FROM QUANTUM SPIN CHAIN: SET THE STAGE

A quantum battery is usually considered as N identical and independent quantum mechanical systems, in arbitrary dimension, expressed by a Hamiltonian, H_0, having nondegenarate eigenvalues. To extract work, the system is driven by an interacting Hamiltonian, acting on the total N-party system, H^g_{charging}, which can, in general, be time-dependent [15–25]. Such Hamiltonian can, in principle, create entanglement in the dynamical state.

In contrast to this, we choose a quantum battery, made up of N interacting spin-$\frac{1}{2}$ particles governed by a Hamiltonian, H_0. In this work, one of our primary goals is to study the effect of interactions and its nature on the efficiency of the battery. Hence the Hamiltonian considered here constitutes of two parts, given by

$$H_0 = H_{\text{field}} + H_{\text{int}}, \tag{1}$$

where H_{field} represents the external local magnetic field, while H_{int} is two- or more-body interactions between the spins of the spin chain. To drive the system (or more precisely, the battery), a local charging field H_{charging}, is applied on each individual spin. See Fig. 1 for the schematic representation of the battery. With $H_{\text{int}} = 0$, the battery and its charging process consist only of local terms, so that it becomes exactly

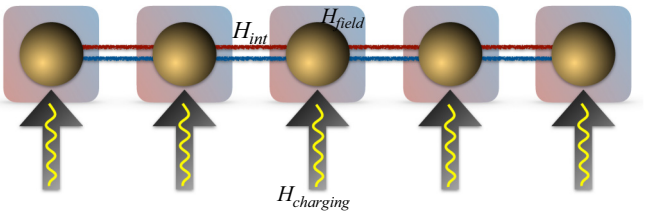

FIG. 1. Schematic diagram of a quantum battery. Initially, the thermal or the ground state of a spin chain, having interaction part, H_{int}, and the local magnetic field part, H_{field}, acts as a quantum battery. It is then driven by the local magnetic field, H_{charging}, to extract maximal power from the battery.

analogous to a situation which cannot possess any quantum features like entanglement or quantum discord. Note that the similar scenario is considered in Ref. [26,27], although unlike the local field, the interacting part of the Hamiltonian along with the charging field is employed to extract the work from the battery.

Let us first notice that one can trivially increase the efficiency of the battery by multiplying some constant (greater than one) to H_0, or by increasing the magnitude of the local part, H_{field}, of the Hamiltonian. To make the analysis nontrivial, we normalize H_0 as

$$\frac{1}{E_{\max} - E_{\min}}[2H_0 - (E_{\max} + E_{\min})\mathbb{I}] \to H_0, \tag{2}$$

where $E_{\min}$ and $E_{\max}$ are minimum and maximum energy eigenvalues of H_0 respectively. Due to this normalization, the spectrum of H_0 is now bounded in $[-1, 1]$ irrespective of the parameter values. This normalization enables us to exactly find the consequence of H_{int} in power compared to the case with vanishing interaction part, i.e., $H_{\text{int}} = 0$, which may not have any quantum characteristics.

The charging of the battery in a closed system takes place according to the unitary operator, given by

$$U(t) = \exp(-iH_{\text{charging}}t), \tag{3}$$

which is responsible for the time evolution of the initial state, $\rho(t = 0)$, of the battery. Initially, the battery is prepared either in (1) the ground state of the normalized Hamiltonian, which corresponds to the situation of absolute zero temperature, or (2) the canonical equilibrium state, $\rho_{th} = \exp(-\beta H_0)/Z$, for a given inverse temperature, $\beta = 1/k_B T$, with $Z = \text{Tr}[\exp(-\beta H_0)]$ and k_B being the corresponding partition function and the Boltzmann constant, respectively. It is important to note here that since the absolute zero temperature is hard to achieve in experiment, a state with finite temperature is a natural choice for the initial state of the battery. At a particular time instant t, the total work output by the battery can be defined as

$$W(t) = \text{Tr}[H_0\rho(t)] - \text{Tr}[H_0\rho(t = 0)], \tag{4}$$

where $\rho(t) = U(t)\rho(t = 0)U(t)^\dagger$ is the evolved state of the system. The corresponding average power for a given time t can be written as $P(t) = \frac{W(t)}{t}$. The aim in preparing the battery is to maximize the extractable power, and hence it is important to choose a proper time when the evolution should be stopped. Towards this objective, the maximum average power obtained

from a given battery can be quantified as

$$P_{\max} = \max_t \frac{W(t)}{t}, \tag{5}$$

where the maximization is performed over time, t. In the rest of the paper, we call $P_{\max}$ the power of the battery, which is the maximum power, obtained in optimized time.

We use exact diagonalization techniques to obtain the ground (or thermal) states as well as the evolved states. For optimization over time, t, we first use global optimization algorithms (simulated annealing and straightforward grid method), and then employ the widely used COBYLA local optimization algorithm [93].

III. QUANTUM SPIN MODEL AS BATTERY

Let us describe the properties of quantum XYZ Heisenberg spin chain with magnetic field which we consider as H_0. Its ground or canonical equilibrium state serves as the possible initial state of the battery. The Hamiltonian consisting of N spin-1/2 particles with an open boundary condition reads as

$$H_0 = \underbrace{\frac{1}{2}h\sum_{j=1}^{N}\sigma_j^z}_{H_{\text{field}}} + \underbrace{\frac{1}{4}\sum_{j=1}^{N-1}J_j\left[(1+\gamma)\sigma_j^x\otimes\sigma_{j+1}^x + (1-\gamma)\sigma_j^y\otimes\sigma_{j+1}^y\right] + \frac{1}{4}\sum_{j=1}^{N-1}\Delta_j\sigma_j^z\otimes\sigma_{j+1}^z}_{H_{\text{int}}}, \tag{6}$$

where σ^α ($\alpha = x, y, z$) represents the usual Pauli spin matrices, h is the strength of the external magnetic field at each site, $0 \leqslant \gamma \leqslant 1$ is the anisotropy constant, and $\{J_j\}$, $\{\Delta_j\}$ are the nearest-neighbor coupling constants in the xy plane and in the z direction, respectively. They may or may not depend on site j. In a closed system, the quantum battery can be charged by applying local external magnetic field in the x direction with strength ω, as

$$H_{\text{charging}} = \frac{\omega}{2}\sum_{j=1}^{N}\sigma_j^x. \tag{7}$$

To obtain the work and then power of the battery, the time dynamics is computed by constructing the unitary operator via Eq. (7) where the ground or the thermal state of the spin model in Eq. (6) is used as the initial state. It is important to stress here that realizability of these models by currently available technologies creates possibilities to implement the proposed battery in laboratories.

A. Quantum XYZ Heisenberg model with homogeneous interaction

Depending on the scenarios, whether the sets $\{J_j\}$ or $\{\Delta_j\}$ is site-independent or not, the spin system can be called ordered or disordered. In this paper, we will explore both cases. Let us first consider the system with $J_j = J$ and $\Delta_j = \Delta$, i.e. the parameters involved in Eq. (6) are site-independent, leading to the ordered spin chain. In one dimension, Eq. (6) represents a paradigmatic family of Hamiltonians with nearest-neighbor interactions, having a rich phase diagram at zero temperature. Let us now discuss some important subclasses of H_0, and their phase portraits:

(1) $\Delta = 0$ and $\gamma \geqslant 0$ [94–96]: $\gamma = 0$ represents the transverse XX spin chain, while the XY spin model having transverse magnetic field is with $\gamma \neq 0$. They belong to two different universality classes: the former one has a *gapless* spin-liquid (SL) phase for $|J/h| > 1$ and a paramagnetic (PM) phase for $|J/h| < 1$, while the later one belongs to the Ising universality class, consisting of a PM ($|J/h| < 1$), an antiferromagnetic (AFM) ($J/|h| > 1$), and a ferromagnetic (FM) ($J/|h| < -1$) phase. Both models can be solved analytically by Jordan-Wigner transformations [94–96] for arbitrary system size including in the thermodynamic limit.

(2) $\gamma = 0$, $\Delta \neq 0$ [97–99]: The model is known as the XXZ spin chain. For $h = 0$, the model is integrable: with $J = 1$, there is an AFM region for $\Delta > 1$, and $\Delta < -1$ corresponds to the ferromagnetic (FM) one, while $-1 < \Delta < 1$ is the gapless SL phase. By using different approximate and numerical techniques, quantum critical lines and their corresponding phases of the system with $h \neq 0$ have also been explored [97]. For example, with small values of magnetic field and Δ, a new phase, Néel order in the y direction, develops, which is known as spin-flop (SF) phase.

(3) $\Delta \neq 0$, $\gamma \geqslant 0$ (XYZ model) [100–102]: The model is not exactly solvable. Several numerical and approximate studies of the XYZ model with field reveal that it has a very rich phase diagram. In particular, like the XXZ model, it also posses FM, AFM, and SF phases, although for nonzero values of γ, two new quantum phase transitions [103,104] of different kinds appear: one from SF to a new phase called a gapless floating phase (FP), while another one is from the FP to the AFM phase.

We will show in the next section that tuning parameters leading to different quantum spin models play an essential role in building and maintaining the performance of the battery.

B. Quantum XYZ model with random interaction strength: Disordered quantum spin model

Let us now consider the system, in which one of the interaction strengths is chosen randomly. It can be found during the preparation process of the materials or due to dislocations of atoms from their regular lattice sites or due to environmental effects [105–109]. Since the change of disorder in these systems remains almost fixed for certain times, specifically a much longer duration than that of the evolution of the system, this kind of disorder can be called "quenched," which we will consider in this paper. It can also be created and controlled in laboratories with cold atoms in optical lattices, linear chains of ions, etc. [65–70]. In this paper, two situations are considered:

(1) The nearest-neighbor exchange interaction in the xy plane, $\{J_j/|h|\}$, are randomly chosen from a Gaussian distribution with mean $\overline{J}/|h|$ and the standard deviation σ_J, which we refer as the strength of disorder. $\sigma_J = 0$ corresponds to the ordered case. Here $\{\Delta_j/|h|\} = \Delta/|h|$ remains independent of the sites. Quenched averaging is performed by first computing the power of the battery for each realization with random-distributed $\{J_j/|h|\}$ and then by taking the average over all realizations. Mathematically, for a physical quantity, $\mathcal{O}$, and for a randomly chosen parameter, $\{X_j\}$, with mean $\overline{X}$ and standard deviation σ_X involved in the system, the quenched averaged quantity can be represented as

$$\langle O(\overline{X}, \sigma_X)\rangle = \iint \cdots \int \mathcal{O}\{X_j\} d\{X_j\}, \tag{8}$$

where the integration is carried out with respect to the probability distribution by which the $\{X_j\}$ are chosen. In our case, the power of the quantum battery ($P_{\max}$) is the physical quantity, which has to be quenched averaged over the parameter space, $\{J_j/|h|\}$, denoted by $\langle P_{\max}\rangle$.

(2) Fixing $\{J_j/|h|\} = J/|h|, \forall j$, we also study the effect of disorder on power by choosing $\{\Delta_j/|h|\}$ randomly from a Gaussian distribution with mean $\overline{\Delta}/|h|$ and standard deviation σ_Δ.

IV. INTERACTION ENHANCES THE POWER: ORDERED CASE

In this section we address the question whether nearest-neighbor interactions can be beneficial for increasing the extraction of power from the battery. To demonstrate this, we first consider the ground state as the initial state of the quantum ordered XY model with transverse magnetic field as the battery, and then move on to the role of interactions in the z direction by considering the XYZ model. We further study the effects of finite temperature on the efficiency.

A. Effects of interaction term in the XY model

Let us consider the ground state of the transverse XY model and compute the power, $P_{\max}$, with the variation of $J/|h|$ for fixed values of system size, N. The behavior of power, depicted in Fig. 2(a), shows that the battery prepared by using an interacting Hamiltonian has higher power as output for certain system parameters than that of the system without interactions. For demonstration, we fix some values of γ and the strength of the charging field as $\omega = 2|h|$. The interesting observations in the pattern of $P_{\max}$ are listed below:

(1) *Positive vs negative interaction strength.* Positive and negative coupling constants, i.e., $J/|h| > 0$ and $J/|h| < 0$, indicate the nature of interaction to be antiferomagnetic (AFM) and ferromagnetic (FM) ones. As depicted in Fig. 2(a), we observe that $P_{\max}$ increases when $0 < J/|h| \lesssim 1$ and reaches its maximum value close to $J/|h| \approx 1$, while it decreases for $J/|h| < 0$. Typically, static physical quantities, like magnetization, classical correlators and entanglement [14], in the ground state are symmetric across $J/|h| = 0$-line [30,31,110]. The asymmetry observed here arises due to the choice of uniform charging field in the x direction, given in Eq. (7), and also the battery Hamiltonian, H_0. Specifically, when

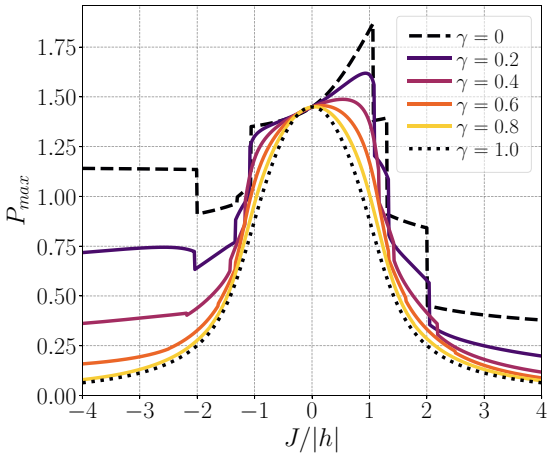

FIG. 2. $P_{\max}$ (ordinate) vs $J/|h|$ (abcissa). $P_{\max}$ is computed for the transverse XY model (i.e., $\Delta/|h| = 0$) with different values of the anisotropy parameter, γ. Here $N = 8$. In the paper, all plots are for the same system size, unless mentioned otherwise. Both axes are dimensionless.

interaction strength is large, $|J/h| > 1$, the initial state is either in the AFM phase or in the FM phase where spins are oriented in the x direction for higher values of γ. Now, since the charging field is in the x direction, it can easily drive the system without demanding more energy, leading to a low amount of power generation. On the other hand, when $|J/h| < 1$, i.e. in the PM phase, spins have affinity towards the z direction due to the external field. Therefore, the charging Hamiltonian needs more energy to drive the system out of equilibrium, thereby leading to a high amount of power in this phase. However, the pattern of $P_{\max}$ clearly establishes that the interaction of H_0 helps to improve the performance of the battery in the paramagnetic phase of the XY model. It is clear from the Fig. 3(b) that for any values of anisotropy parameter ($0 \leqslant \gamma < 1$), power gets increased in presence of interaction in the PM phase. So, in terms of the enhancement of power,

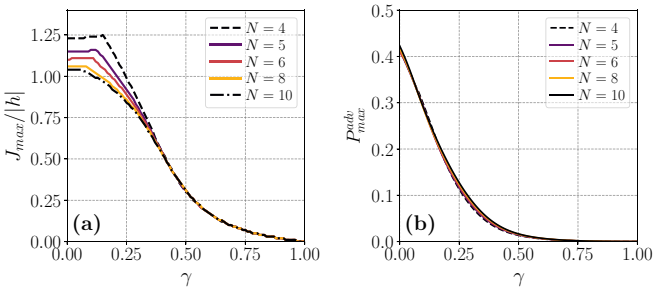

FIG. 3. Dependence of $P_{\max}$ on the interaction strength and the anisotropy parameter, γ. Plots are for different system sizes and $\Delta = 0$. (a) $J_{\max}/|h|$ vs γ. $J_{\max}/|h|$ represents the interaction strength for which $P_{\max}$ reaches its maximum value for a given value of γ and N. Note that for higher values of γ, $J_{\max}/|h|$ does not depend on N. (b) $P_{\max}^{\text{adv}}$ vs γ. The advantages in power due the introduction of XY-exchange couplings are measured by the quantity $P_{\max}^{\text{adv}} = P_{\max}(J_{\max}/|h|) - P_{\max}(J/|h| = 0)$. Interestingly, $P_{\max}^{\text{adv}}$ becomes scale-invariant for the entire range of γ. Both axes are dimensionless.

we find that the observation is independent of the anisotropy parameter (γ).

(2) *Dependence on* γ. Although the increment of power of the battery is independent of the anisotropy parameter, the magnitude of enhancement, however, depends on γ. To be precise, maximal power of the battery greatly depends on the anisotropy parameter, as is evident from Fig. 2(a). Among all the γ values, if the battery is initially in the ground state of the XX model having $\gamma = 0$, the power output is maximum, as compared to the other values of γ. Also, from Fig. 2(a), we find that the range of $J/|h|$, where the advantage in power can be obtained, shrinks with increasing γ. The reason behind this feature is the same as stated in the previous point, that, with increasing γ, the strength of exchange interaction in the y direction decreases, and as a result, the tendency to align (or antialign) in the y direction also decreases. Therefore, it continuously becomes easier for the charging Hamiltonian to drive the system. To visualize the γ dependence, we identify the interaction strength, $J/|h|$, for which $P_{\max}$ reaches its maximum value, which we refer to as $J_{\max}/|h|$. We then investigate the behavior of $J_{\max}/|h|$ with γ for different system sizes, as shown in Fig. 3(a).

(3) *Role of exchange interaction: Scale invariance.* The interaction part, H_{int}, in H_0 is important in $P_{\max}$ as already discussed. To quantify its influence, we introduce a quantity,

$$P_{\max}^{\text{adv}} = P_{\max}(J_{\max}/|h|) - P_{\max}(J/|h| = 0), \tag{9}$$

where $P_{\max}(J_{\max}/|h|)$ and $P_{\max}(J/|h| = 0)$ are, respectively, power measured at $J_{\max}/|h|$ defined above and at $J/|h| = 0$. $P_{\max}^{\text{adv}}$ reaches its maximum value at $\gamma = 0$ and decreases with the increase of γ as seen in Fig. 3(b). Specifically, we find that when $\gamma = 0$, a nonvanishing interaction, in the chain of $N = 8$ sites, can produce up to 28.8% increase in power, thereby showing the relevance of a quantum battery. Note, however, that for $\gamma = 1$, we find that $P_{\max}^{\text{adv}} = 0$, i.e., the local scenario is most efficient, and interaction does not help. Importantly, we observe that $P_{\max}^{\text{adv}}$ does not depend on the number of spins in the chain, showing the *scale invariance* property of the advantage.

(4) *Quantum phase transition signaled through power.* The second-order quantum phase transition [41,111,112] in the XY model at zero temperature can be detected by the first derivatives of several physical quantities, which include correlation length [41], entanglement [14], quantum discord [113,114], etc. Since $P_{\max}$ is measured in the evolution, it is not *a priori* clear that it can identify quantum phase transitions. We here show that for low values of γ, the dynamical quantity, $P_{\max}$ itself, can signal quantum phase transition by showing a finite jump around $|J/h| \approx 1$. For higher values of γ, $P_{\max}$ changes its curvature from concave to convex so that its derivative shows the kink. It is interesting to note here that in a different context of dynamical phase transition [71,72], a quantity like Loschmidt echo defined as the distance between the ground and the evolved states of the quantum spin model can also mimic the equilibrium phase transition. Our results, therefore, suggest that it will be interesting to find (some) other dynamical quantities, similar to power output, which can also carry the information about the equilibrium phases of the initial systems.

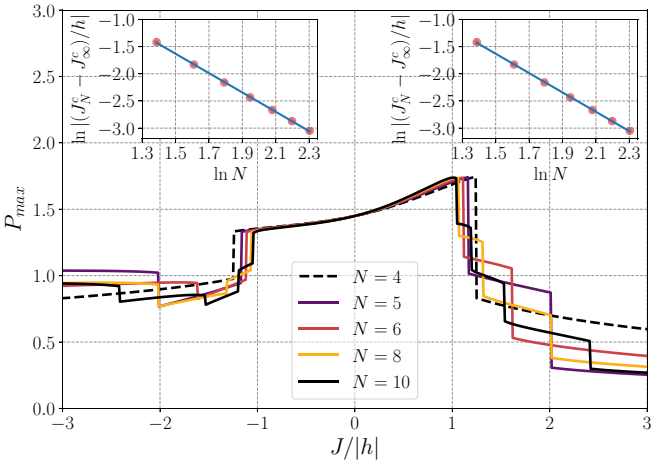

FIG. 4. Dependence of power on system size, N, for $\gamma = 0.1$ and $\Delta = 0$. We plot the variation of $P_{\max}$ with $J/|h|$ for different system size, N. (Insets) Finite-size scaling of the critical points, $J_N^c/|h|$, as indicated by the power. We plot $\ln|(J_N^c - J_\infty^c)/h|$ (both numerical data and fitted lines) as functions of $\ln N$ for FM $\leftrightarrow$ PM (left inset) and AFM $\leftrightarrow$ PM (right inset) transitions. Both axes are dimensionless.

(5) *Dependence of power on N.* With the variation of N, we observe that in the range $-1 \lesssim J/|h| \lesssim 1$, the power does not change its behavior substantially. However, $J_{\max}/|h|$, which leads to maximum $P_{\max}$ shifts towards $J/|h| = 1$ with the increase of N, although the value of the maximum power, as well as maximum advantage in power, remain almost unaltered with N (see Figs. 3 and 4). This is possible because the curvature of $P_{\max}$ becomes steeper with N. On the other hand, finite-size effects on $P_{\max}$ are visible for $J/|h| < -1$ as well as for $J/|h| > 1$ [Figs. 2(a) and 4].

(6) *Scaling.* Since power of the battery can detect equilibrium quantum phase transition as discussed above, it is now natural to ask about the scaling law followed by it. Ambitiously, we find the finite-size scaling of critical points, as indicated by the behavior of $P_{\max}$, as

$$\left|\frac{(J_N^c - J_\infty^c)}{h}\right| = 1.039 \times N^{-1.78}, \tag{10}$$

for both FM $\leftrightarrow$ PM and AFM $\leftrightarrow$ PM transitions for $\gamma = 0.1$ [Fig. 4 (insets)]. Here $J_N^c/|h|$ is computed where the power shows a first jump for a fixed value of N, while $J_\infty^c/|h| = 1$ as known for the transverse quantum XY model in the thermodynamic limit. The reason for choosing the first jump in the evaluation of scaling is discussed in Appendix. Note, moreover, that we possibly should not compare the scaling exponent obtained above with the other indicators of QPT: (1) other physical quantities detecting QPT are calculated in the ground states while the power output is found in dynamics, and the above study establishes that even the dynamical quantity can also carry information about QPT; and (2) the system sizes simulated are too small to demand any comparison.

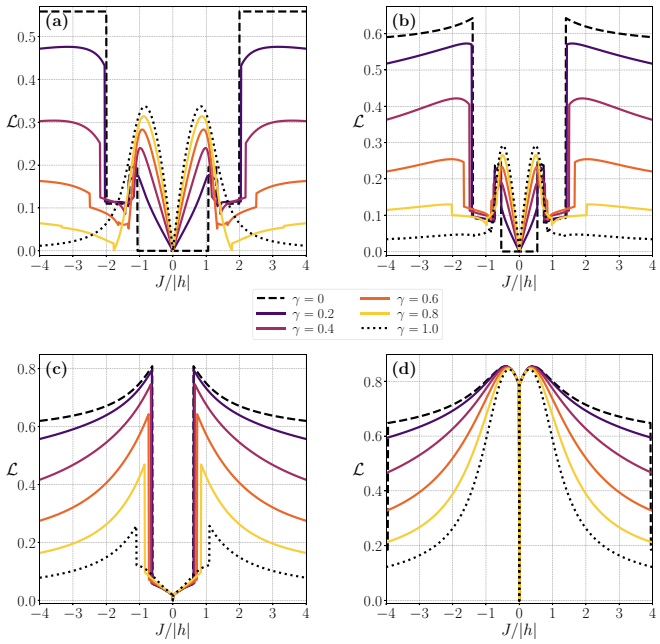

FIG. 5. Plot of nearest-neighbor entanglement of the ground state in the XYZ model having different values of γ with the variation of $J/|h|$ (x axis). Plots are for specific values of the interaction strengths in the z direction, $\Delta/|h|$, as mentioned in the headings of each plot. We observe that entanglement is symmetric with $J/|h| = 0$, which is not the case for $P_{\max}$ (comparing Figs. 2 and 6), although the patterns for both of them are qualitatively similar in some regions for $\gamma > 0$. Hence one can argue that entanglement can be a necessary ingredient for good quantum battery, but not sufficient.

B. Role of entanglement

We have already shown that many-body interactions can increase the efficiency of a quantum battery. Let us now ask a natural question: *does interspin entanglement play any role in the performance of the battery?* To answer this query, we compute bipartite entanglement [14] of the reduced density matrix obtained by tracing out all the parties except two from the middle of the chain of both the initial state and the state at the time when $P_{\max}$ is optimized. We take the pair of spins from the middle of the chain to minimize any boundary effects due to the open boundary condition. In particular, we calculate logarithmic negativity [115], which is the modulus of the negative eigenvalue of the partial transposed state for two spin-1/2 particles [116,117].

Let us first consider the XY model. If one compares Figs. 5(a) and 2 with $J/|h| > 0$, we find that the nearest-neighbor entanglement qualitatively mimics the features of $P_{\max}$—it increases in regions $-1 \lesssim J/|h| < 0$ as well as $0 \lesssim J/|h| < 1$ and then decreases with $J/|h|$ for different values of $\gamma \neq 0$. Such characteristics indicates that entanglement can be a necessary ingredient to extract more power, but not sufficient, which is in parity with the earlier results (see Ref. [25] and references therein).

C. Introduction of interaction in z direction leads to enhancement in power

Let us now move to the XYZ model with magnetic field, given in Eq. (6). We will address the question whether the additional interactions in the z direction, i.e., the model with $\Delta/|h| \neq 0$, are required to increase the power of the battery. As before, the battery is initially prepared as the ground state of this model.

Comparing Fig. 6 with Fig. 2, we find that with the increase of $\Delta/|h|$, the power increases in the region of $J/|h| < 0$ where the power was decreasing in the absence of $\Delta/|h|$, thereby establishing the usefulness of the coupling in the z direction. Moreover, we observe that for moderate values of $\Delta/|h|$, there is a lower bound on the coupling constant in the xy plane, denoted by $J_c/|h| < 0$, where $P_{\max}$ increases beyond the value obtained with the initial state of the battery being the ground state of the Hamiltonian without any XY exchange interaction, i.e., with $J/|h| = 0$. Note, however, that the model with $J/|h| = 0$ and $\Delta/|h| \neq 0$ corresponds to the system having nonvanishing interactions, since the field, given to drive the system, is in the complementary direction of the exchange interaction of the parent Hamiltonian. Again, with the increase of γ, $J_c/|h|$ decreases, although it is much bigger than that obtained for the XY model. It shows that even if the tuning of the system parameters cannot be performed properly, the XYZ model is more appropriate to build the quantum battery than the XY model.

Although the XYZ model has several competing factors which lead to the generation of high power from the battery, there can be a physical explanation along the same lines discussed for the XY model. With nonzero $\Delta/|h|$, spins gain another competing tendency, which is to antialign themselves in the z direction. In the PM phase of the XY model with $J/|h| < 0$, we do not find any enhancement. However, with the introduction of $\Delta/|h|$ along with the field in the z direction, the charging field in the x direction possibly requires more energy to drive the system out of equilibrium, resulting in more power.

D. Effect of temperature on power of the battery

We have already shown that the zero-temperature state as the initial state of an interacting Hamiltonian is advantageous for generating a high amount of power in the quantum battery. We will now see whether such improvement persists (or even increases) when the initial state is the thermal state, ρ_{th}, having a finite temperature. This is important because in the laboratory, absolute zero temperature is not easy to obtain. To produce power, a local charging Hamiltonian, in Eq. (7), is again applied to each site. As one expects, we see that $P_{\max}$ vanishes for infinite temperature, i.e., for $\beta = 0$, then starts increasing as β increases, and finally saturates to the power of the zero temperature. However, we notice that the variation of $P_{\max}$ with increasing β is not always monotonic, and can have one or more *nonmonotonic bumps* depending on the system parameter, which signifies that we can have situations where the battery performs more efficiently at higher temperature than the lower ones. More interestingly, and quite counter-intuitively, it turns out that battery may output more power at finite temperature than that of the absolute zero temperature.

Quantitatively, we consider a quantity which can capture the advantages gained at finite temperature over the zero temperature, given by

$$P_{\max}^{T-\text{diff}} = P_{\max}(T > 0) - P_{\max}(T = 0), \tag{11}$$

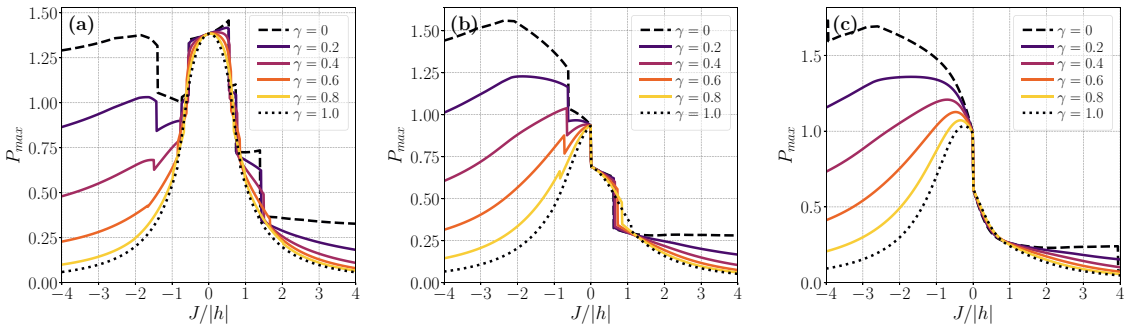

FIG. 6. $P_{\max}$ (vertical) vs $J/|h|$ (horizontal) for the quantum XYZ Heisenberg model with different values of γ. Plots are for specific values of the interaction strengths in the z direction, $\Delta/|h|$, as mentioned in the headings of each plot. Both axes are dimensionless.

where $P_{\max}(T > 0)$ and $P_{\max}(T = 0)$ are the extractable power obtained with the thermal state and with the ground state, respectively. Indeed, we find that $P_{\max}^{T-\text{diff}}$ is positive for certain choices of $J/|h|$ and $\beta/|h|$ [see Fig. 7 for four sets of values of $(\Delta/|h|, \gamma)$], thereby showing the gain of choosing the thermal state as an initial state. Numerical simulations also confirm that changing system parameters does not alter the results qualitatively.

V. DISORDER-ENHANCED POWER FROM THE BATTERY

In this section we examine how the presence of impurities in interactions can induce power generation by the battery. The observations are mainly classified into two situations: (1) random XY exchange interactions, i.e., randomly chosen Gaussian-distributed $\{J_j/|h|\}$, keeping $\{\Delta_j/|h|\} = \Delta/|h|$ fixed for all sites, and (2) disorder in $\{\Delta_j/|h|\}$, with $\{J_j/|h|\} = J/|h|$ being site-independent. In general, impurities reduce the physical properties like magnetization, conductivity in systems [32–34], and hence the performance of the tasks. However, we report that both disordered cases considered here can deliver some advantages: (1) disorder enhances power generation over the ordered case for suitably chosen system parameters, i.e., disorder-induced order; and (2) increment in the interaction strength of the disordered case leads to a more increase in the power than that of the ordered one. It implies that the curvature of quenched averaged power, $\langle P_{\max}\rangle$, in the model with random interactions has a sharper increase towards the maximum than the system without any impurities.

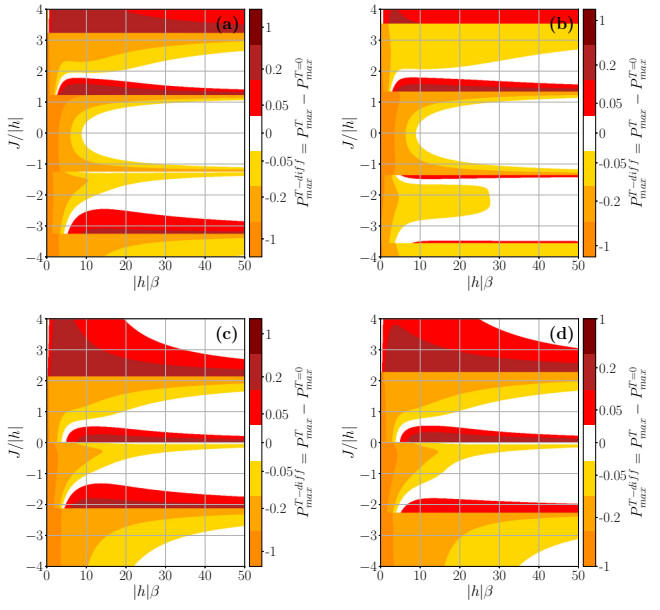

FIG. 7. Map of $P_{\max}^{T-\text{diff}}$ (see Sec. IV D for definition) with respect to $|h|\beta$ (abscissa) and $J/|h|$ (ordinate). Here $N = 4$. (a)–(b) For the XY model with two different values of γ, $\gamma = 0$ and $\gamma = 0.4$; (c) and (d) the behavior for the XYZ model with $\Delta/|h| = 1$ and the same values of γ as in (a) and (b). Positivity of $P_{\max}^{T-\text{diff}}$ indicates the advantage of considering initial state at finite temperature, while the negative values of $P_{\max}^{T-\text{diff}}$ show the benefit for the ground states. Both axes are dimensionless.

A. Effects of randomness in XY-exchange interaction

Let us concentrate on the first scenario with $\{\Delta_j/|h|\} = \Delta/|h|$ and the disorder in $\{J_j/|h|\}$, chosen from the Gaussian distribution with a given mean, $\overline{J}/|h|$, and a standard deviation, σ_J. As mentioned in Sec. III B, to obtain the quenched averaged value of the power, we here perform averaging over 5000 realizations, which we find to be sufficient to converge $\langle P_{\max}\rangle$ up to a second decimal place. Below we emphasize our primary observations regarding the effects of randomness in XY couplings as depicted in Fig. 8.

(1) For $\Delta/|h| = 0$, i.e., for the transverse XY model, increasing the mean interaction strength, $|\overline{J}/|h|$, from $\overline{J}/|h| = 0$, does not help to increase the maximum power over the ordered scenario [Figs. 8(a) and 8(b)]. On the other hand, for given values of system parameters, there are situations, in both the $\overline{J}/|h| > 0$ and $\overline{J}/|h| < 0$ regions, where increasing disorder strength, σ_J, results in better production of power, $\langle P_{\max}\rangle$, than that in the ordered case, thereby showing disorder-induced power output. Such advantages are prominent for lower values of the anisotropy parameter, γ, and negative values of $\overline{J}/|h|$ [Figs. 8(a) and 8(b)].

(2) Interestingly, in the presence of strong and constant interaction in the z direction [e.g., when $\Delta/|h| = 1$ as shown in Figs. 8(c) and 8(d)], we find that for $\overline{J}/|h| < 0$, there are situations where we can get better quenched averaged power output by increasing $|\overline{J}/|h|$ than the one obtained in the ordered XYZ model. Second, for fixed values of system parameters, $|\overline{J}/|h|$, a battery produces more power with the increase of σ_J. Specifically, we observe that there exist regions

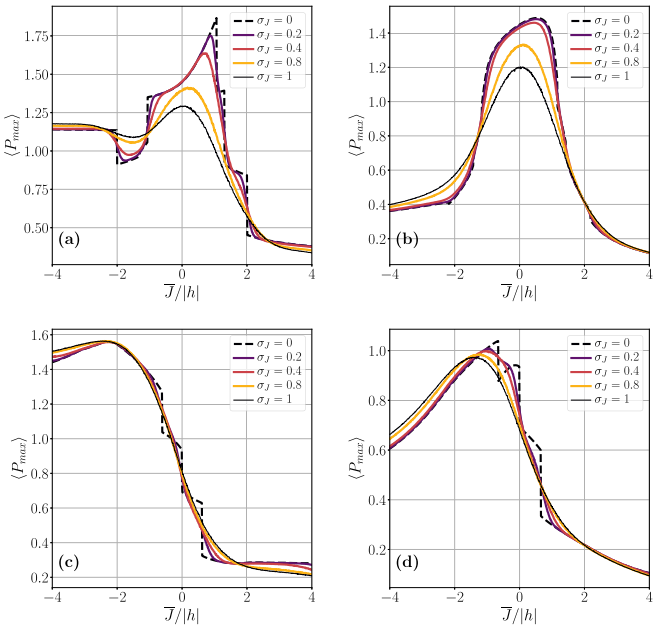

FIG. 8. Quenched averaged power, $\langle P_{\max}\rangle$, vs $\overline{J}/|h|$ for different disorder strength σ_J. Note that $\sigma_J = 0$ refers to the ordered case. Disorder is introduced in the coupling constant in the xy plane, $J_j/|h|$, for fixed values of $\Delta/|h|$ and γ. The choices of $\Delta/|h|$ and γ are the same as in Fig. 7. The twin advantages mentioned in the text can be visualized from the plots with $\Delta/|h| \neq 0$. Both axes are dimensionless.

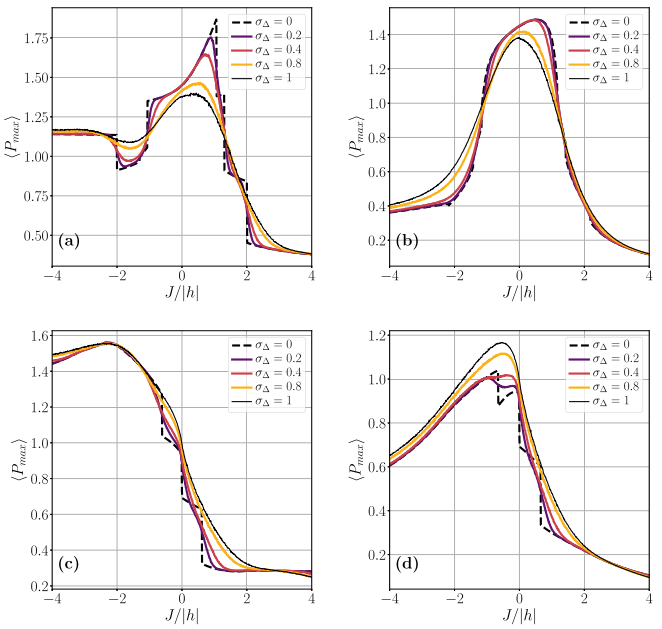

FIG. 9. $\langle P_{\max}\rangle$ with $J/|h|$ for specific choices of mean $\overline{\Delta}/|h|$ and the anisotropy parameter, γ. Plots show the effects of disorder in the interaction, $\{\Delta_j\}$, in the z direction, on the power for different disorder strength, σ_Δ. The choices of $\overline{\Delta}/|h|$ and γ are the same as in Fig. 7. Both axes are dimensionless.

in $|\overline{J}/h|$ where $\langle P_{\max}\rangle$ with $\sigma_J = 1$ produces maximum power than any other values of σ_J. Moreover, as shown in all situations, an increase in the anisotropy parameter suppresses the power generation from the battery.

B. Effects of impurities in the interaction strength in the z direction

Let us now move to the case where randomness is introduced in the interaction strength in the z direction, i.e., $\{\Delta_j/|h|\}$ are taken randomly from Gaussian distribution with mean, $\overline{\Delta}/|h|$, and standard deviation, σ_Δ, keeping $\{J_j/|h|\} = J/|h|$ fixed for every sites (Fig. 9). As before, we take 5000 different realizations for quenching.

Comparing Figs. 9(a) and 9(b) with Figs. 8(a) and 8(b), we safely claim that the pattern of $\langle P_{\max}\rangle$ for model with $\overline{\Delta}/|h| = 0$ is almost identical to the disordered transverse XY model. Note that $\overline{\Delta}/|h| = 0$ refers to the disordered XYZ model and does not correspond to the XY model.

However, it turns out that the Hamiltonian with $\overline{\Delta}/|h| > 0$ is much more beneficial (see Fig. 9) as compared to the previous cases, where randomness was in $\{J_j/|h|\}$ and when $\overline{\Delta}/|h| = 0$. Two prominent differences between these two types of disordered scenarios are as follows:

(1) Advantages in power with increasing disorder strength and fixed values of system parameters are less affected by increasing γ than any previous situations considered in this paper. Instead of diminishing the power, we find that the moderate values of γ lead to more efficiency in power production of the battery in the presence of strong disorder.

(2) With nonzero $\overline{\Delta}/|h|$, we observe that the quenched averaged power increases with the variation of σ_Δ for the entire region of $|J/h|$, thereby showing advantages of systems having impurities for preparing a quantum battery. In particular, as seen in Fig. 9(d) with $\overline{\Delta}/|h| = 1$ and $\gamma = 0.4$, $\sigma_\Delta = 1$ generates maximum quenched power, $\langle P_{\max}\rangle$, than do any other values of σ_Δ. As argued before for the XY and the XYZ models, this kind of advantage can also be explained as follows: We choose $\bar{\Delta}/|h| = 1$, from a Gaussian distribution with mean unity and standard deviation σ_Δ, which implies that the value of $\Delta/|h|$ is approximately between $1 - 3\sigma_\Delta$ and $1 + 3\sigma_\Delta$. Thus the nonvanishing nearest-neighbor interaction along with the magnetic field in the z direction dominates over the xy coupling, which is not possible in the XY model, and hence the driving field in the x direction requires more energy to take out the system from equilibrium, thereby producing more power.

Such a phenomenon of having the advantage of a disordered system over the clean case can be referred to as disorder-induced order observed in dynamics.

VI. CONCLUSION

Batteries convert chemical energy to electrical energy, thereby accomplishing our high demands for electricity in daily life. On the other hand, technological developments lead to the devices, which are smaller and smaller in size, and hence the effects of quantum mechanics on them are inevitable. Moreover, it was discovered that quantum-based technologies are more efficient than the existing classical ones. Therefore, it is natural to explore whether storage

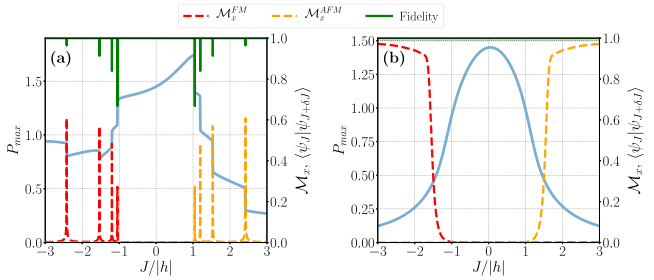

FIG. 10. Order parameters $\mathcal{M}_x^{\mathrm{FM}}$ and $\mathcal{M}_x^{\mathrm{AFM}}$ and the fidelity $\langle\psi_J|\psi_{J+\delta J}\rangle$ for $N = 10$ and $\gamma = 0.1,\ 0.8$. Here we take $\delta J = 0.005|h|$. The order parameters have nonzero finite values in the corresponding ordered phases, which may not be easily visible in the plots for $\gamma = 0.1$.

devices can also be improved by using quantum mechanics. It was recently found that this is indeed the case.

If we build a quantum battery which is initially prepared in the ground or thermal states of the quantum spin chain, the power extracted via local external magnetic field is higher for the interacting models than the noninteracting ones. In particular, we illustrate the usefulness of an interacting Hamiltonian by considering the ground state of the transverse XY and the XYZ model with magnetic field as the initial state of the battery. We observe that performance of the battery in terms of producing power declines with the increase of γ. Specifically, the best model which demonstrates the maximum efficiency is the transverse XX model. Although natural intuition says that the performance of a device can decline with the increase of temperature, we find that the suitable tuning of system parameters leads to a scenario where maximal power generation is higher with the initial state prepared at finite temperature than the state with absolute zero temperature. Finally, we report that impurities help to improve the generation of quenched averaged power from the battery built up using the ground state of the XYZ model with random couplings either in the xy plane or in the z direction in comparison with the ordered systems—a phenomenon known as disorder-induced order. Both the presence of impurities and finite temperature are unavoidable in experiments. Hence the enhancement obtained in both cases indicates that the implementation of the battery is possible even when the control over the system is not adequate.

ACKNOWLEDGMENTS

The authors thank Ujjwal Sen for fruitful discussions. T.C. acknowledges support of the National Science Centre (Poland) via QuantERA Programme No. 2017/25/Z/ST2/03029.

APPENDIX

Let us briefly discuss in detail the consequence of finite jumps observed in Fig. 2. In this respect, let us first note that finite jumps can occur only for low values of the anisotropy parameter γ, where interactions in the x and y directions have comparable strengths. Since we are working with very small systems ($N = 4, 6, 8, 10$), the quantum fluctuations are typically large, and the exchange interactions face problems

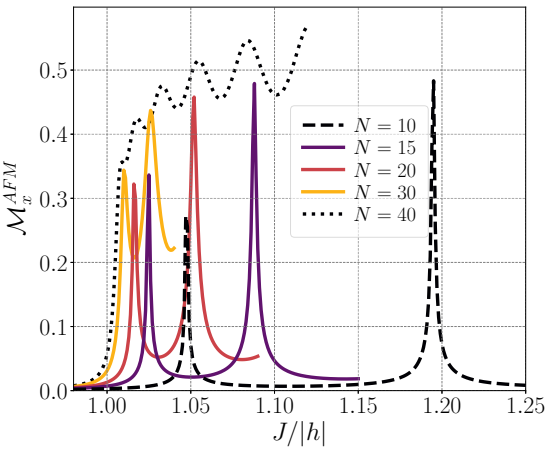

FIG. 11. Order parameter $\mathcal{M}_x^{\mathrm{AFM}}$ for $\gamma = 0.1$ and $N = 10, 15, 20, 30, 40$.

to align (or antialign) the spins along some specific directions in the xy plane when the value of γ is small. That is why the transition points at $J/|h| = \pm 1$ get bifurcated into different points which correspond to the finite jumps in the power curve.

We can confirm this by calculating the ferromagnetic and antiferromagnetic order parameters

$$\mathcal{M}_x^{\mathrm{FM}} = \sum_j \langle\sigma_x\rangle /N$$

and

$$\mathcal{M}_x^{\mathrm{AFM}} = \sum_j (-1)^j \langle\sigma_x\rangle /N,$$

respectively, as well the fidelity $\langle\psi_J|\psi_{J+\delta J}\rangle$ (see Fig. 10). Clearly, the finite jumps in power occur exactly at the same positions where the order parameters show nonanalyticity and the fidelity shows a dip from $\approx$1. Hence, we can argue that all jumps technically correspond to the phase transition point, which have been bifurcated from the thermodynamic point due to finite-size effects. On the other hand, for high values of γ, say, 0.8, such a problem cannot persist, since in that case, interaction in the x direction dominates compared to that in the y direction, and spins can easily align (or antialign) in the x direction.

To clarify such finite-size effects further, we compute same order parameter for larger system sizes. For example, in Fig. 11 we observe the first two nonanalytic points in $\mathcal{M}_x^{\mathrm{AFM}}$ for $N = 10, 15, 20, 30$, and first few for $N = 40$. Clearly, with increasing system size, all nonanalytic points become smoother, and the second one approaches (as well as the later ones also) the first one and ultimately merges into one. Therefore, we can expect that the first nonanalytic point approaches the thermodynamic value, i.e., $J/|h| = 1$, and hence we consider the first jump in the analysis of scaling.

For the plots, we employ an exact diagonalization method and density matrix renormalization group [118–123] technique. For calculating order parameters, we add a uniform (or staggered) field of magnitude $10^{-4}|h|$ in the x direction to the Hamiltonian to break the Z_2 symmetry.

[1] M. Nielsen and I. Chuang, *Quantum Computation and Quantum Information* (Cambridge University Press, Cambridge, 2000).

[2] J. M. Raimond, M. Brune, and S. Haroche, Rev. Mod. Phys. **73**, 565 (2001).

[3] J. W. Pan, Z. B. Chen, C. Y. Lu, H. Weinfurter, A. Zeilinger, and M. Zukowski, Rev. Mod. Phys. **84**, 777 (2012).

[4] D. Leibfried, R. Blatt, C. Monroe, and D. Wineland, Rev. Mod. Phys. **75**, 281 (2003).

[5] H. Hafner, C. F. Roose, and R. Blatt, Phys. Rep. **469**, 155 (2008).

[6] K. Singer, U. Poschinger, M. Murphy, P. Ivanov, F. Ziesel, T. Calarco, and F. Schmidt-Kaler, Rev. Mod. Phys. **82**, 2609 (2010).

[7] L.-M. Duan and C. Monroe, Rev. Mod. Phys. **82**, 1209 (2010).

[8] I. Bloch, Nat. Phys. **1**, 23 (2005).

[9] I. Bloch, J. Dalibard, and W. Zwerger, Rev. Mod. Phys. **80**, 885 (2008).

[10] J. Simon *et al.*, Nature (London) **472**, 307 (2011).

[11] R. Barends *et al.*, Nature (London) **508**, 500 (2014).

[12] C.- P. Yang, Q.-P. Su, S.-B. Zheng, and F. Nori, New J. Phys. **18**, 013025 (2016).

[13] T. Baumgratz, M. Cramer, and M. B. Plenio, Phys. Rev. Lett. **113**, 140401 (2014).

[14] R. Horodecki, P. Horodecki, M. Horodecki, and K. Horodecki, Rev. Mod. Phys. **81**, 865 (2009).

[15] R. Alicki and M. Fannes, Phys. Rev. E **87**, 042123 (2013).

[16] K. V. Hovhannisyan, M. Perarnau-Llobet, M. Huber, and A. Acin, Phys. Rev. Lett. **111**, 240401 (2013).

[17] F. C. Binder, S. Vinjanampathy, K. Modi, and J. Goold, New J. Phys. **17**, 075015 (2015).

[18] J. Jaramillo, M. Beau, and A. del Campo, New J. Phys. **18**, 075019 (2016).

[19] F. Campaioli, F. A. Pollock, F. C. Binder, L. Ceĺeri, J. Goold, S. Vinjanampathy, and K. Modi, Phys. Rev. Lett. **118**, 150601 (2017).

[20] D. Ferraro, M. Campisi, G. M. Andolina, V. Pellegrini, and M. Polini, Phys. Rev. Lett. **120**, 117702 (2018).

[21] N. Friis and M. Huber, Quantum **2**, 61 (2018).

[22] G. M. Andolina, M. Keck, A. Mari, V. Giovannetti, and M. Polini, Phys. Rev. B **99**, 205437 (2019).

[23] D. Farina, G. M. Andolina, A. Mari, M. Polini, and V. Giovannetti, Phys. Rev. B **99**, 035421 (2019).

[24] G. M. Andolina, M. Keck, A. Mari, M. Campisi, V. Giovannetti, and M. Polini, Phys. Rev. Lett. **122**, 047702 (2019).

[25] F. Campaioli, F. A. Pollock, and S. Vinjanampathy, arXiv:1805.05507.

[26] T. P. Le, J. Levinsen, K. Modi, M. M. Parish, and F. A. Pollock, Phys. Rev. A **97**, 022106 (2018).

[27] G. M. Andolina, D. Farina, A. Mari, V. Pellegrini, V. Giovannetti, and M. Polini, Phys. Rev. B **98**, 205423 (2018).

[28] D. S. Jin and J. Ye, Phys. Today **64**(5), 27 (2011).

[29] I. M. Georgescu, S. Ashhab, and F. Nori, Rev. Mod. Phys. **86**, 153 (2014).

[30] M. Lewenstein, A. Sanpera, V. Ahufinger, B. Damski, A. Sen(De), and U. Sen, Adv. Phys. **56**, 243 (2007).

[31] M. Lewenstein, A. Sanpera, and V. Ahufinger, *Ultracold Atoms in Optical Lattices: Simulating Quantum Many Body Physics* (Oxford University Press, Oxford, 2012).

[32] P. W. Anderson, Phys. Rev. **109**, 1492 (1958).

[33] E. Abrahams, P. W. Anderson, D. C. Licciardello, and T. V. Ramakrishnan, Phys. Rev. Lett. **42**, 673 (1979).

[34] P. A. Lee and T. V. Ramakrishnan, Rev. Mod. Phys. **57**, 287 (1985).

[35] V. Ahufinger, L. Sanchez-Palencia, A. Kantian, A. Sanpera, and M. Lewenstein, Phys. Rev. A **72**, 063616 (2005).

[36] L. Fallani, C. Fort, and M. Inguscio, Adv. At. Mol. Opt. Phys. **56**, 119 (2008).

[37] A. Aspect and M. Inguscio, Phys. Today **62**(8), 30 (2009).

[38] L. S.-Palencia and M. Lewenstein, Nat. Phys. **6**, 87 (2010).

[39] G. Modugno, Rep. Prog. Phys. **73**, 102401 (2010).

[40] B. Shapiro, J. Phys. A **45**, 143001 (2012).

[41] S. Sachdev, *Quantum Phase Transitions* (Cambridge University Press, Cambridge, 2011).

[42] M. C. Arnesen, S. Bose, and V. Vedral, Phys. Rev. Lett. **87**, 017901 (2001).

[43] X. Wang, Phys. Rev. A **66**, 034302 (2002).

[44] G. L. Kamta and A. F. Starace, Phys. Rev. Lett. **88**, 107901 (2002).

[45] S. Scheel, J. Eisert, P. L. Knight, and M. B. Plenio, J. Mod. Opt. **50**, 881 (2003).

[46] F. K. Fumania, S. Nematib, S. Mahdavifar, and A. H. Daroonehb, Physica A (Amsterdam) **445**, 256 (2016).

[47] T. Chanda, T. Das, D. Sadhukhan, A. K. Pal, A. Sen(De), and U. Sen, Phys. Rev. A **94**, 042310 (2016).

[48] T. Chanda, T. Das, D. Sadhukhan, A. K. Pal, A. Sen(De), and U. Sen, Phys. Rev. A **97**, 012316 (2018).

[49] T. Giamarchi and H. J. Schulz, Phys. Rev. B **37**, 325 (1988).

[50] M. P. A. Fisher *et al.*, Phys. Rev. B **40**, 546 (1989).

[51] R. T. Scalettar, G. G. Batrouni, and G. T. Zimanyi, Phys. Rev. Lett. **66**, 3144 (1991).

[52] W. Krauth, N. Trivedi, and D. Ceperley, Phys. Rev. Lett. **67**, 2307 (1991).

[53] A. Sanpera, A. Kantian, L. Sanchez-Palencia, J. Zakrzewski, and M. Lewenstein, Phys. Rev. Lett. **93**, 040401 (2004).

[54] D. Chowdhury, *Spin Glasses and Other Frustrated Systems* (Wiley, New York, 1986).

[55] M. Mezard, G. Parisi, and M. A. Virasoro, *Spin Glass Theory and Beyond* (World Scientific, Singapore, 1987).

[56] J. P. Álvarez Zúñiga and N. Laflorencie, Phys. Rev. Lett. **111**, 160403 (2013).

[57] Z. Yao, K. P. C. da Costa, M. Kiselev, and N. Prokofev, Phys. Rev. Lett. **112**, 225301 (2014).

[58] M. Znidaric, T. Prosen, and P. Prelovsek, Phys. Rev. B **77**, 064426 (2008).

[59] A. Pal and D. A. Huse, Phys. Rev. B **82**, 174411 (2010).

[60] E. Canovi, D. Rossini, R. Fazio, G. E. Santoro, and A. Silva, Phys. Rev. B **83**, 094431 (2011).

[61] J. H. Bardarson, F. Pollmann, and J. E. Moore, Phys. Rev. Lett. **109**, 017202 (2012).

[62] J. Eisert, M. Friesdorf, and C. Gogolin, Nat. Phys. **11**, 124 (2015).

[63] A. Auerbach, *Interacting Electrons and Quantum Magnetism* (Springer, New York, 1994).

[64] B. Rosenstein and D. Li, Rev. Mod. Phys. **82**, 109 (2010).

[65] D. Clément, A. F. Varón, M. Hugbart, J. A. Retter, P. Bouyer, L. Sanchez-Palencia, D. M. Gangardt, G. V. Shlyapnikov, and A. Aspect, Phys. Rev. Lett. **95**, 170409 (2005).

[66] C. Fort, L. Fallani, V. Guarrera, J. E. Lye, M. Modugno, D. S. Wiersma, and M. Inguscio, Phys. Rev. Lett. **95**, 170410 (2005).
[67] J. Billy *et al.*, Nature (London) **453**, 891 (2008).
[68] G. Roati *et al.*, Nature (London) **453**, 895 (2008).
[69] L. Fallani, J. E. Lye, V. Guarrera, C. Fort, and M. Inguscio, Phys. Rev. Lett. **98**, 130404 (2007).
[70] M. White, M. Pasienski, D. McKay, S. Q. Zhou, D. Ceperley, and B. DeMarco, Phys. Rev. Lett. **102**, 055301 (2009).
[71] M. Heyl, A. Polkovnikov, and S. Kehrein, Phys. Rev. Lett. **110**, 135704 (2013).
[72] M. Heyl, Phys. Rev. Lett. **113**, 205701 (2014).
[73] A. Aharony, Phys. Rev. B **18**, 3328 (1978).
[74] D. E. Feldman, J. Phys. A **31**, L177 (1998).
[75] B. J. Minchau and R. A. Pelcovits, Phys. Rev. B **32**, 3081 (1985).
[76] I. A. Fomin, J. Low Temp. Phys. **134**, 97 (2005).
[77] I. A. Fomin, JETP Lett. **85**, 434 (2007).
[78] G. E. Volovik, JETP Lett. **81**, 647 (2005).
[79] D. A. Abanin, P. A. Lee, and L. S. Levitov, Phys. Rev. Lett. **98**, 156801 (2007).
[80] G. E. Volovik, J. Low Temp. Phys. **150**, 453 (2008).
[81] A. Niederberger, T. Schulte, J. Wehr, M. Lewenstein, L. Sanchez-Palencia, and K. Sacha, Phys. Rev. Lett. **100**, 030403 (2008).
[82] S. Lellouch, T. L. Dao, T. Koffel, and L. Sanchez-Palencia, Phys. Rev. A **88**, 063646 (2013).
[83] A. Niederberger, J. Wehr, M. Lewenstein, and K. Sacha, Europhys. Lett. **86**, 26004 (2009).
[84] R. L. Greenblatt, M. Aizenman, and J. L. Lebowitz, Phys. Rev. Lett. **103**, 197201 (2009).
[85] A. Niederberger, M. M. Rams, J. Dziarmaga, F. M. Cucchietti, J. Wehr, and M. Lewenstein, Phys. Rev. A **82**, 013630 (2010).
[86] A. Niederberger, B. A. Malomed, and M. Lewenstein, Phys. Rev. A **82**, 043622 (2010).
[87] P. Lugan and L. Sanchez-Palencia, Phys. Rev. A **84**, 013612 (2011).
[88] M. Aizenman, R. L. Greenblatt, and J. L. Lebowitz, J. Math. Phys. **53**, 023301 (2012).
[89] R. Prabhu, S. Pradhan, A. Sen (De), and U. Sen, Phys. Rev. A **84**, 042334 (2011).
[90] U. Mishra *et al.*, New J. Phys. **18**, 083044 (2016).
[91] D. Sadhukhan *et al.*, New J. Phys. **17**, 043013 (2015).
[92] D. Sadhukhan, S. S. Roy, D. Rakshit, R. Prabhu, A. SenDe, and U. Sen, Phys. Rev. E **93**, 012131 (2016).
[93] M. J. D. Powell, Acta Numerica **7**, 287 (1998).
[94] E. Lieb, T. Schultz, and D. Mattis, Ann. Phys. (NY) **16**, 407 (1961).
[95] E. Barouch, B. M. McCoy, and M. Dresden, Phys. Rev. A **2**, 1075 (1970).
[96] E. Barouch and B. M. McCoy, Phys. Rev. A **3**, 786 (1971).
[97] D. V. Dmitriev, V. Ya. Krivnov, and A. A. Ovchinnikov, Phys. Rev. B **65**, 172409 (2002), and references therein.
[98] G. Müller and R. E. Shrock, Phys. Rev. B **32**, 5845 (1985).
[99] M. Takahashi, *Thermodynamics of One-Dimensional Solvable Models* (Cambridge University Press, Cambridge, 1999).
[100] P. Bak, Rep. Prog. Phys. **45**, 587 (1982).
[101] E. Sela, A. Altland, and A. Rosch, Phys. Rev. B **84**, 085114 (2011).
[102] F. Pinheiro, G. M. Bruun, J.-P. Martikainen, and J. Larson, Phys. Rev. Lett. **111**, 205302 (2013).
[103] J. M. Kosterlitz and D. J. Thouless, J. Phys. C **6**, 1181 (1973).
[104] J. M. Kosterlitz, J. Phys. C **7**, 1046 (1974).
[105] M. Guo, R. N. Bhatt, and D. A. Huse, Phys. Rev. Lett. **72**, 4137 (1994).
[106] H. Rieger and A. P. Young, Phys. Rev. Lett. **72**, 4141 (1994).
[107] H. Rieger, in *Quantum Annealing and Other Optimization Methods*, edited by A. Das and B. K. Chakrabarti, Lecture Notes in Physics Vol. 679 (Springer, Berlin, 2005).
[108] F. Fernandez-Alonso and D. L. Price (Eds.), *Neutron Scattering–Magnetic and Quantum Phenomena*, Experimental Methods in the Physical Sciences Vol. 48 (Elsevier, 2015).
[109] T. Vojta, Annu. Rev. Condens. Matter Phys. **10**, 233 (2019), and references therein.
[110] L. Amico, R. Fazio, A. Osterloh, and V. Vedral, Rev. Mod. Phys. **80**, 517 (2008).
[111] B. K. Chakrabarti, A. Dutta, and P. Sen, *Quantum Ising Phases and Transitions in Transverse Ising Models* (Springer, Heidelberg, 1996).
[112] S. Suzuki, J.-I. Inou, and B. K. Chakrabarti, *Quantum Ising Phases and Transitions in Transverse Ising Models* (Springer, Heidelberg, 2013).
[113] K. Modi, A. Brodutch, H. Cable, T. Paterek, and V. Vedral, Rev. Mod. Phys. **84**, 1655 (2012).
[114] A. Bera *et al.*, Rep. Prog. Phys. **81**, 024001 (2018).
[115] G. Vidal and R. F. Werner, Phys. Rev. A **65**, 032314 (2002).
[116] A. Peres, Phys. Rev. Lett. **77**, 1413 (1996).
[117] M. Horodecki, P. Horodecki, and R. Horodecki, Phys. Lett. A **223**, 1 (1996).
[118] S. R. White, Phys. Rev. Lett. **69**, 2863 (1992).
[119] S. R. White, Phys. Rev. B **48**, 10345 (1993).
[120] G. Vidal, Phys. Rev. Lett. **91**, 147902 (2003).
[121] G. Vidal, Phys. Rev. Lett. **93**, 040502 (2004).
[122] U. Schollwöck, Rev. Mod. Phys. **77**, 259 (2005).
[123] U. Schollwöck, Ann. Phys. **326**, 96 (2011).